CHEMISTRY
A EUROPEAN JOURNAL

DOI: 10.1002/chem.201001333

Hierarchical Tin Oxide Octahedra for Highly Efficient Dye-Sensitized Solar Cells

Yu-Fen Wang, Jian-Wen Li, Yuan-Fang Hou, Xiao-Yun Yu, Cheng-Yong Su, and Dai-Bin Kuang*[a]

Since the great breakthrough made in 1991 by O'Regan[1] and Grätzel[2], dye-sensitized solar cells (DSSCs) have attracted tremendous interest and are becoming one of the most promising candidates for practical photovoltaic applications due to their low production cost and efficient photovoltaic performance. Up to now, more than 11% power conversion efficiency has been reported for DSSCs based on TiO_2 nanocrystalline photoelectrodes.[3] It is well known that the composition and structure of the photoelectrode material play an important role in the photovoltaic performance and stability of DSSCs. As an efficient photoelectrode, the material should have a large surface area to adsorb larger amounts of dye and highly ordered nanoarrays or densely packed microstructure for fast electron transport and light scattering.[4–6] Among the photoelectrodes, one interesting structure is the double-layer electrode containing a dye adsorption layer (10–15 μm thick, consisting of ≈20 nm particles) and a light-scattering layer (3–5 μm thick, consisting of a few hundreds of nanometer particles); this has been found to improve the photovoltaic performance.[7] Another novel photoelectrode is the hierarchically structured film consisting of submicron spheres that are made up of 10–20 nm particles. The photoelectrode consists of this kind of bifunctional material with both the dye adsorption layer (nanoparticles) and the light-scattering layer (submicron spheres), which results in a significant enhancement of power conversion efficiency.[5,6] However, most of the works have been only focused on the hierarchical TiO_2 or ZnO spheres.[5,6] Tin oxide, as an n-type semiconductor with a wide direct band gap of 3.6 eV at 300 K,[8] is one of the promising multifunctional materials in gas sensors,[9] dye-sensitized solar cells,[10] lithium ion batteries, and so on.[11] SnO_2 nanoparticles and hollow SnO_2 microspheres have been reported to exhibit about 5% photovoltaic performance.[10] However, to the best of our knowledge, hierarchically structured octahedral (nonspherical) SnO_2 materials have not yet been reported for DSSCs applications; this might be an ideal structure because the eight faces at the submicron level can have a light-scattering effect.

Herein, we report, for the first time, a rapid and facile sonochemical process to synthesize uniform octahedral $Sn_6O_4(OH)_4$ intermediates, resulting in hierarchical SnO_2 octahedra approximately 1.0 μm in size, consisting of SnO_2 nanoparticles about 30 nm in diameter by heat treatment of the as-made $Sn_6O_4(OH)_4$ at 800 °C for 3 h in air. The reaction solution containing $SnCl_2{\cdot}2H_2O$ (1.128 g), diethanolamine (5.0 mL), diethylene glycol (DEG, 40 mL), and deionized water (10 mL) is subjected to intense ultrasonic irradiation for 10 min; the resulting precipitates were collected by centrifugation at 5000 rpm for 5 min. The present sonochemical method has a few clear advantages over traditional hydrothermal processes, such as it is simple, fast, low energy cost, and does not require surfactants or templates.[12,13] The hierarchical SnO_2 octahedra consisting of nanoparticles were further used as photoelectrodes for DSSC applications, showing a highly efficient power conversion efficiency of 6.40%.

Figure 1a shows the typical XRD patterns of samples prepared by a sonochemical reaction for 10 min (curve I) and further heat treatment at 800 °C for 3 h (curve II). As shown in curve I, the well-resolved peaks can be indexed to the tetragonal structure $Sn_6O_4(OH)_4$ (JCPDS card no. 46-1486) with cell constants of $a=b=7.927$ and $c=9.102$ Å. After calcination of the as-prepared samples, all intense diffraction peaks (curve II) are in good agreements with rutile-like tetragonal structure of SnO_2 (JCPDS card no. 41-1445) with cell constants of $a=b=4.738$ and $c=3.187$ Å. It shows that n-type SnO_2 semiconductor powders are obtained through

[a] Y.-F. Wang, J.-W. Li, Y.-F. Hou, X.-Y. Yu, Prof. C.-Y. Su, Prof. D.-B. Kuang
MOE Key Laboratory of Bioinorganic and Synthetic Chemistry
State Key Laboratory of Optoelectronic Materials and Technologies
School of Chemistry and Chemical Engineering
Sun Yat-Sen University, Guangzhou 510275 (P. R. China)
Fax: (+86) 20-8411-3015
E-mail: kuangdb@mail.sysu.edu.cn

Supporting information for this article is available on the WWW under http://dx.doi.org/10.1002/chem.201001333.

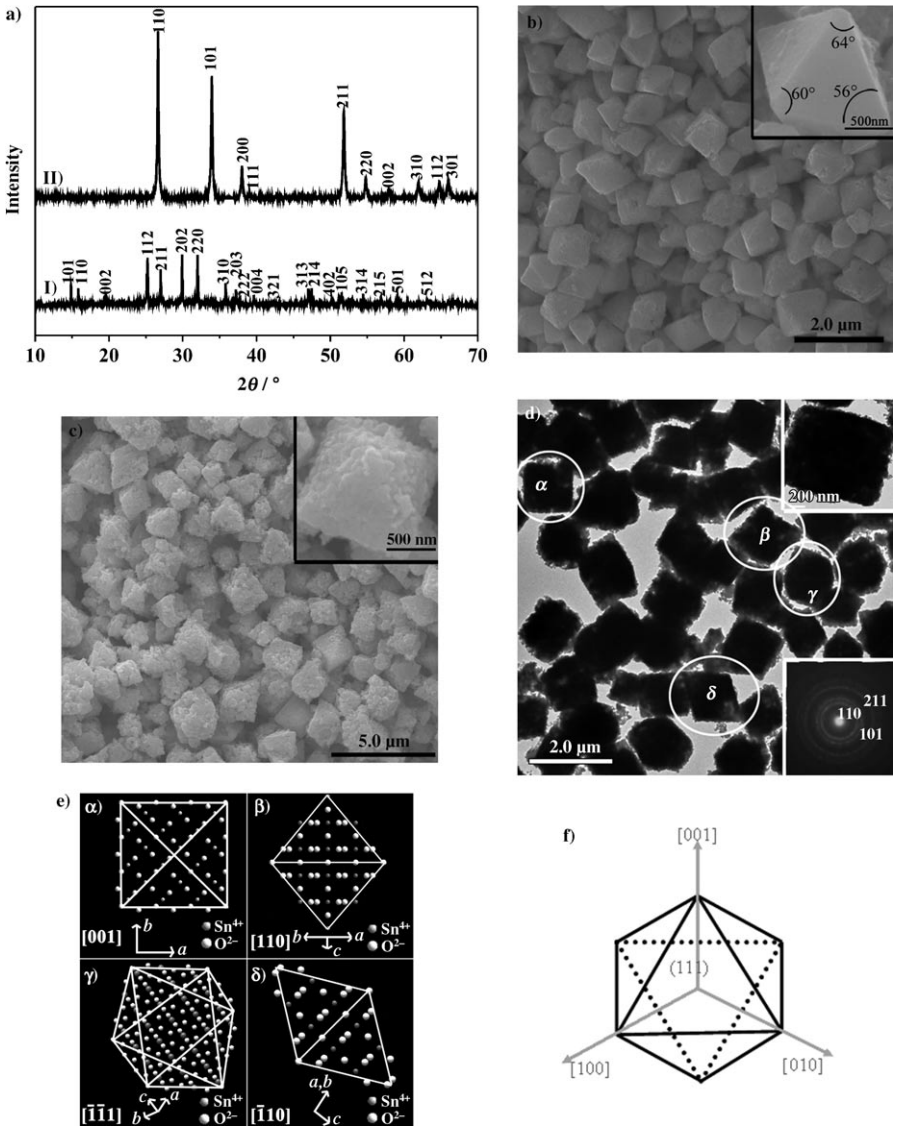

Figure 1. a) Powder X-ray diffraction patterns of as-synthesized $Sn_6O_4(OH)_4$ sample after sonochemical reaction for 10 min (curve I) and SnO_2 octahedra with a heat treatment at 800 °C for 3 h (curve II). b) and c) are the FE-SEM images of as-prepared $Sn_6O_4(OH)_4$ octahedra and calcined hierarchical octahedral SnO_2, respectively. Insets in b) and c) are the high-magnification FE-SEM images of $Sn_6O_4(OH)_4$ and SnO_2, respectively. d) TEM image of SnO_2 octahedra. Upper and lower insets are an individual SnO_2 octahedron and the corresponding diffraction pattern, respectively. e) Schematic models of an ideal SnO_2 octahedron projected in different directions: α): [001], β): [110] ,γ): [$\bar{1}\bar{1}$1], δ): [$\bar{1}$10], which are related to the SnO_2 octahedron marked in Figure 1 d. f) Model of an ideal octahedron.

the oxidization and decomposition of as-prepared $Sn_6O_4(OH)_4$ during calcination.

The morphology of the as-prepared $Sn_6O_4(OH)_4$ and calcined SnO_2 was characterized by field-emission scanning electron microscopic (FE-SEM), shown in Figure 1 b and c, respectively. It is interesting to note that the uniform $Sn_6O_4(OH)_4$ octahedra were easily observed after the simple and fast sonochemical reaction (10 min). The $Sn_6O_4(OH)_4$ octahedron has eight very smooth equilateral triangles faces with an average edge length of 1.0 μm, and the dihedral angle for each set of two conjoined faces were measured to be about (60 ± 1), (56 ± 1),and (64 ± 1)°, respectively, which are close to the theoretic value (60°) of an octahedron. After heat treatment of the as-prepared octahedral $Sn_6O_4(OH)_4$ at 800 °C for 3 h, the hierarchical SnO_2 octahedra consisting of nanoparticles were observed, shown in Figure 1 c. The octahedral morphology of SnO_2 remains constant even after calcination. The rough surface clearly reveals the hierarchical SnO_2 octahedra are composed of nanoparticles approximately 30 nm in diameter (inset in Figure 1 c).

The octahedral SnO_2 were further characterized by TEM, high-resolution TEM (HRTEM), and selected-area electron diffraction (SAED) analyses, as shown in Figure 1 d and Figure S1 in the Supporting Information. The low-magnification TEM image (Figure 1 d) clearly reveals the octahedral structure of SnO_2 sample. Several SnO_2 octahedra are marked by α, β, γ, and δ, which are viewed along [001], [110], [$\bar{1}\bar{1}$1], and [$\bar{1}$10] directions, respectively. Their morphological characters are in good agreements with the corresponding schematic modes of octahedral SnO_2, projected along the same direction (Figure 1 e). The SAED pattern of an individual SnO_2 octahedron reveals it is a polycrystallite (inset in Figure 1 d, lower right). Figure S1 in the Supporting Information further reveals the hierarchical SnO_2 octahedron is composed of SnO_2 particles of approximately 30 nm. The HRTEM image shows the SnO_2 nanoparticles are single crystalline and the distances of lattice fringes were determined to be 0.333 and 0.267 nm, which can be indexed as (110) and (101) planes, respectively. The ideal model of SnO_2 octahedral shape (Figure 1 f) shows each face is a capped triangle-based pyramid, and the SnO_2 crystal is bound by eight {111} faces.[14] In fact, each octahedron has eight triangles and the overall structure shares 12 identical edges.

To investigate the formation mechanism of octahedral $Sn_6O_4(OH)_4$ during the present sonochemical process, time-dependent experiments were performed and the products

were monitored by FE-SEM observations. Figure S2 in the Supporting Information displays a series of interesting images that show the morphological evolution of products synthesized at different sonication times (from 0 to 3 min). Without sonication (0 min), the products prepared after mixing $SnCl_2{\cdot}2H_2O$ and diethanolamine in a solvent mixture of DEG and water are nanoparticles (Figure S2a). After sonication for 1 min, the primary nanoparticles connected to each other assemble into nanorod and dendritic structures (Figure S2b). With the prolongation of the sonication reaction (3 min), the irregular $Sn_6O_4(OH)_4$ octahedra consisting of nanoparticles were observed and are shown in Figure S2c. Then, the $Sn_6O_4(OH)_4$ octahedra with smooth crystal faces can be achieved in terms of continuous surface flattening[13] when the sonication reaction increased to 10 min, shown in Figure 1b. Finally, after calcination in air at 800 °C for 3 h, hierarchical SnO_2 octahedra consisting of nanoparticles were obtained by the oxidization and decomposition of octahedral $Sn_6O_4(OH)_4$ intermediates.

According to the FE-SEM observations of the samples made at different sonication times, the possible growth process of octahedral SnO_2 through $Sn_6O_4(OH)_4$ intermediates is proposed and shown in Figure 2. Firstly, $Sn_6O_4(OH)_4$ nanorod and dendritic structures were formed through the self-assembly of nanoparticles, with the prolongation of ultrasonic reaction, rough octahedra consisting of nanoparticles were formed through the aggregation or assembly of nanoparticles, which form further $Sn_6O_4(OH)_4$ octahedra with smooth faces due to the surface flattening during the sonochemical process.[13] Finally, after heat treatment at 800 °C for 3 h, the uniform hierarchical SnO_2 octahedra consisting of nanoparticles were obtained.

Sonication plays a crucial role in the present reproducible synthesis of uniform $Sn_6O_4(OH)_4$ octahedra with high yield because it is a rapid and efficient process. The sonochemical process generates localized hot spots with transient high temperatures of around 5000 °C, pressures of about 1000 atm, and heating as well as cooling rates in excess of $1010\ K\,s^{-1}$, which will accelerate the synthesis of materials.[15] DEG, a modified polyol,[16] probably has dual roles, not only as a solvent but also as a coordination reagent to form Sn complexes, similar to the synthesis of ZnO spheres by a microwave process.[17] Small primary $Sn_6O_4(OH)_4$ nuclei are generated by the hydrolysis of Sn complexes and then nanoparticles assemble through the same crystallographic orientation during the ultrasonic reaction. And the formation process of $Sn_6O_4(OH)_4$ octahedra can be ascribed to the well-known growth mechanism of oriented attachment[18,19] and subsequent surface flattening.[13]

Hierarchical SnO_2 octahedra were further used as photoelectrodes for DSSC applications. For DSSC fabrication, a compact TiO_2 blocking layer ($\approx$300 nm thick consisting of 3–5 nm TiO_2 nanoparticles) was deposited between FTO glass and SnO_2 film by spin-coating (see the Experimental Section). Figure 3a shows the current–voltage (I–V) characteristics of the DSSCs based on various SnO_2 photoelectrodes. It is observed that the J_{sc}, V_{oc} and η are 10.96 mA cm^{-2}, 604 mV and 3.17%, respectively, for the SnO_2 octahedral

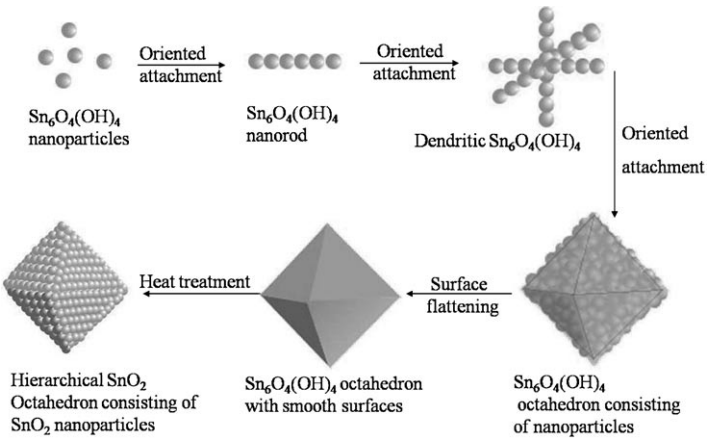

Figure 2. Schematic illustration of the morphology evolution of $Sn_6O_4(OH)_4$ during the sonication and the transformation from $Sn_6O_4(OH)_4$ to SnO_2 during the heat treatment.

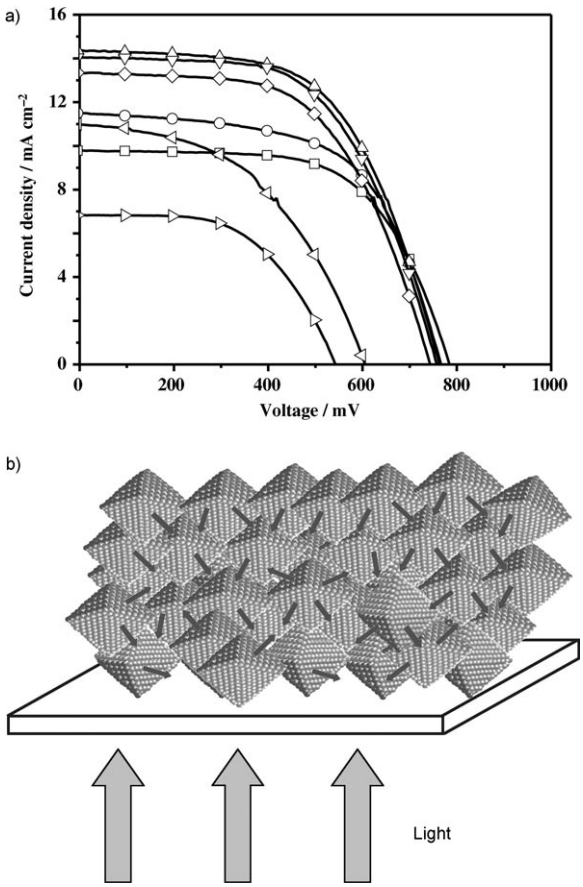

Figure 3. a) Photocurrent density–voltage curves of DSSCs based on hierarchical octahedral SnO_2 films with different thicknesses. □: 6.9, ○: 9.9, △: 13.2, ▽: 16.0, ◇: 18.8, ◁ and ▷: 13.2 μm hierarchical octahedral SnO_2 film. ◁ is without $TiCl_4$ treatment and ▷ is without both TiO_2 blocking layer and $TiCl_4$ treatment. b) Scheme of the SnO_2 film consisting of hierarchical SnO_2 octahedra ($\approx$1 μm in size) that are made of SnO_2 nanoparticles approximately 30 nm in diameter.

photoelectrode with TiO_2 blocking layer, which are much higher than that of 6.84 mA cm^{-2}, 543 mV, 2.07% for the electrode without TiO_2 blocking layer. The introduction of TiO_2 blocking layer was believed to effectively reduce the charge recombination at the FTO/electrolyte hence to improve the photocurrent density, photovoltage and power conversion efficiency.[20] In addition, the higher density of the compact TiO_2 blocking layer, together with larger contact area and improved adherence between the SnO_2 octahedra and FTO surface provides more electron pathways from SnO_2 film to FTO glass, which is helpful for electron transfer and subsequently enhances the electron transfer efficiency. The influence of $TiCl_4$ treatment on the photovoltaic parameters is further investigated. After the $TiCl_4$ treatment of the SnO_2 photoelectrodes, it is found that the photocurrent density and photovoltage increase from 10.96 mA cm^{-2} to 14.39 mA cm^{-2}, and 604 mV to 763 mV, respectively, resulting in a significant improvement of power conversion efficiency from 3.17% to 6.40%. The similar trend is also observed for the nanoparticles based DSSCs (Figure S3, Table S1). This can be ascribed to the significant reduction of the electron-hole recombination via the $TiCl_4$ treatment. The TiO_2 coating the SnO_2 surface will minimize defects at this internal surface, enabling ease of electron transfer from the TiO_2 to the SnO_2 and also avoid any extra internal trap sites which would otherwise be present in a poorly constructed junction.[21] Moreover, recent researches for both liquid and solid state solar cells based on SnO_2 photoelectrode also supported our present results.[10a,21]

Furthermore, the effects of SnO_2 film thickness on the photovoltaic performance are also investigated. The current-voltage (I-V) characteristics of the DSSCs based on hierarchical octahedral SnO_2 photoelectrodes with different thicknesses are shown in Figure 3a and the detailed photovoltaic parameters are summarized in Table 1. As shown in Figure 3a and Table 1, the short-circuit photocurrent density (J_{sc}) varied from 9.77 to 14.39 to 13.34 mA cm^{-2}, with a film thickness increase from 6.9 to 13.2 to 18.8 μm, accompanied with an increase in adsorbed dye amounts. The open-circuit voltage (V_{oc}) decreases with the increasing film thickness, due to the augmentation of the surface area providing additional charge-recombination sites and enhancing the dark current.[7] Moreover, for thicker films the outer SnO_2 particle layers do not contribute significantly to the photogeneration of conduction band electrons due to the filtering of light by the dyed particles located close to the FTO glass.[7] The sharing of photoinjected conduction band electrons by these particles lowers their quasi-Fermi level and hence the V_{oc}. The power conversion efficiency (η) of the solar cells increases from 4.79 to 6.40% and then decrease to 5.69% with the variations in film thickness.

Table 1. Detailed photovoltaic parameters (J_{sc}, V_{oc}, FF, and η) of dye-sensitized SnO_2 solar cells with different film Thicknesses of hierarchical octahedral SnO_2 photoelectrodes.

Film thickness [μm]	J_{SC} [mA cm^{-2}]	V_{OC} [mV]	FF [%]	η [%]	Adsorbed dye [×10^{-8} mol cm^{-2}]
6.9	9.77	784	62.5	4.79	4.99
9.9	11.50	766	59.9	5.28	5.43
13.2	14.39	763	58.3	6.40	6.30
13.2[a]	10.96	604	47.9	3.17	5.30
13.2[b]	6.84	543	56.0	2.07	3.42
16.0	14.05	757	58.2	6.19	6.51
18.8	13.34	744	56.9	5.69	7.93
13.4[c]	12.24	726	58.6	5.21	13.47

[a] Hierarchical octahedral SnO_2 film without $TiCl_4$ treatment. [b] Hierarchical octahedral SnO_2 film without both TiO_2 blocking and $TiCl_4$ treatment. [c] SnO_2 nanoparticle film synthesized by a sonochemical process in 50 mL aqueous solution containing $SnCl_2{\cdot}2H_2O$ (1.128 g) and diethanolamine (5.0 mL; without DEG).

For comparison, SnO_2 nanoparticles of around 40 nm (Figure S4 in the Supporting Information) have been prepared by a sonochemical process in a 50 mL aqueous solution containing $SnCl_2{\cdot}2H_2O$ (1.128 g) and diethanolamine (5.0 mL without DEG). The photovoltaic parameters of the DSSCs based on SnO_2 nanoparticles are $J_{sc}=12.24$ mA cm^{-2}, $V_{oc}=726$ mV, $FF=58.6$%, and energy conversion efficiency = 5.21% (Table 1). It is worth noting that highly efficiency (6.40%) DSSCs were obtained for the hierarchical SnO_2 octahedra, which is much higher than that of SnO_2 nanoparticles (5.21%). Such high photovoltaic performance is mainly ascribed to the novel bifunctional structure of hierarchical SnO_2 octahedra consisting of nanoparticles, in which SnO_2 nanoparticles (≈30 nm) can adsorb large amounts of dye and submicron octahedra (≈1 μm) can act as the light-scattering layer (shown in Figure 3b), which can significantly improve the photocurrent, voltage, and hence the photovoltaic performance. To the best of our knowledge, this is the first report on hierarchical octahedral SnO_2 material for solar cell applications and shows high power conversion efficiency.

The specific BET surface area of the hierarchical SnO_2 octahedra and nanoparticles are 26.3 and 33.9 m^2 g^{-1}, respectively, obtained from the N_2 adsorption–desorption measurements. Although both the surface area and adsorbed dye amounts of hierarchical SnO_2 octahedra are smaller than the SnO_2 nanoparticles, the photovoltaic performance of DSSC based on the former is much higher than the latter. This can be attributed to the effective light scattering of hierarchical SnO_2 octahedra of 1.0 μm, and which is further characterized by the UV/Vis diffuse reflectance spectroscopy. The UV/Vis diffuse reflectance spectra of hierarchical SnO_2 octahedra and SnO_2 nanoparticle films with and without dye adsorption are shown in Figure 4. For the bare SnO_2 films (without dye adsorption), the reflectance of SnO_2 nanoparticles film is much lower than that of hierarchical SnO_2 octahedra film (Figure 4a), revealing the latter has a higher light-scattering ability than the former, caused by the submicron octahedra, which is in agreement with the previous results for the ZnO submicron spheres and nanoparticles.[6] Furthermore, for the dye/SnO_2 film (Figure 4b), the dye-adsorbed hierarchical SnO_2 octahedra film shows a higher reflectance than the dye-adsorbed SnO_2 nanoparticles film in the long-wavelength region (550–700 nm) because of the light scattering from submicron octahedra. Hence, DSSCs

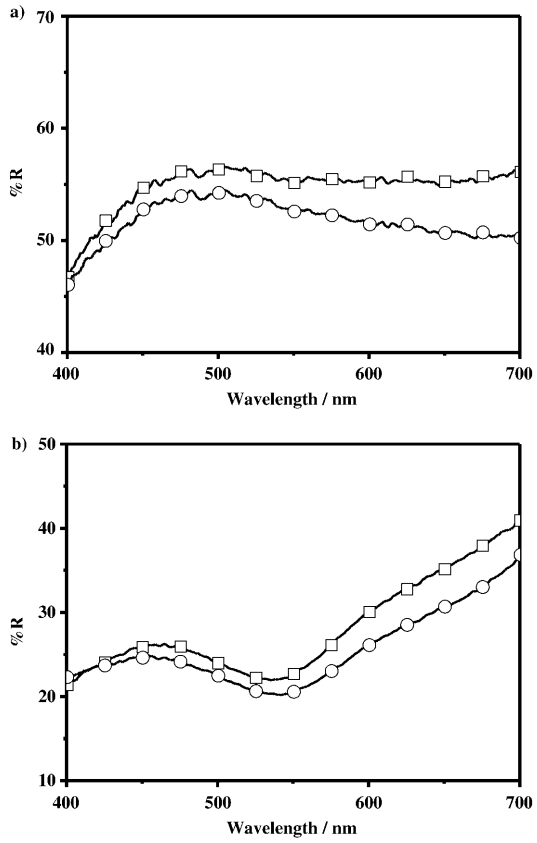

Figure 4. Diffused reflectance spectra of the hierarchical SnO_2 octahedra (□) and SnO_2 nanoparticle films (○) with similar thickness ((13.3 ± 0.1) μm). a) Without, and b) with adsorbed N719 dye.

based on the hierarchical SnO_2 octahedra exhibit superior photocurrent and photovoltaic performance than the SnO_2 nanoparticles, which is mainly attributed to the efficient light scattering for the former.

In summary, well-defined hierarchical SnO_2 octahedra consisting of nanoparticles have been successfully synthesized by a sonochemical process followed by heat treatment. The formation mechanism of octahedral $Sn_6O_4(OH)_4$ can be attributed to an oriented attachment based on time-dependent FE-SEM observations. The hierarchical octahedral SnO_2 shows high power conversion efficiency (6.40%) with a J_{sc} of 14.39 mA cm^{-2} and a V_{oc} of 763 mV under simulated AM 1.5G one sun (100 mW cm^{-2}) illumination for DSSC application. The power conversion efficiency (6.40%) of DSSC based on hierarchical SnO_2 octahedra has a 23% increase compared with that of SnO_2 nanoparticle photoelectrode (5.21%) is mainly ascribed to the efficient light scattering for the former, which is further confirmed by the UV/Vis reflectance spectra.

Experimental Section

Synthesis: In a typical synthesis of $Sn_6O_4(OH)_4$ octahedra intermediates, $SnCl_2{\cdot}2H_2O$ was dissolved in the DEG, after 10 min stirring, deionized water was added to this solution, and it was continuously stirred for 10 min. Afterwards, diethanolamine was added to this solution dropwise and it was stirred for a further 10 min, which resulted in the formation of a white suspension. Subsequently, the suspension was subjected to an intense ultrasonic irradiation (Sonics: VCX-500) for different time. The resulting precipitates were collected by centrifugation at 5000 rpm for 5 min and washed 5 times with absolute ethanol and distilled water, and finally dried at 60 °C for further characterization. To obtain hierarchical SnO_2 octahedra, part of the as-prepared samples were calcined at 800 °C for 3 h in air. For comparison, the synthesis of SnO_2 nanoparticles was also performed in the absence of DEG, while keeping other experimental conditions constant.

Fabrication of SnO_2 paste: Hierarchical SnO_2 octahedra (1.0 g) were ground for 40 min in a mixture of ethanol (8.0 mL), acetic acid (0.2 mL), terpineol (3.0 g), and ethyl cellulose (0.5 g) to form a slurry, and then the mixture was sonicated for 5 min in an ultrasonic bath to form a viscous white SnO_2 paste.

Preparation of the SnO_2 photoelectrode: The cleaned FTO glass (15 Ω/square, Nippon Sheet Glass, Japan) was first spin-coated with a compact TiO_2 blocking layer ≈300 nm thick. The anatase TiO_2 colloidal solution was prepared according to a modified literature procedure.[22] Briefly, titanium *n*-butoxide (34.2 mL) was added slowly to a solution containing acetylacetone (10.2 mL) and *n*-butanol (37.6 mL) under stirring. Hydrolysis of the clear mixture was then performed by the dropwise addition of an aqueous acidic solution (*para*-toluenesulfonic acid (3.8 g) in H_2O (18.0 mL)). Stable transparent TiO_2 (3–5 nm in particle size) was obtained after heating the mixture at 60 °C for 12 h. The hierarchical octahedral SnO_2 paste was screen-printed onto the FTO glass containing the TiO_2 compact layer. The thickness of the SnO_2 film was easily controlled by repeated different screen-printing times. The SnO_2 films were gradually heated under an air flow at 325 °C for 5 min, at 375 °C for 5 min, at 450 °C for 15 min, and then at 500 °C for 15 min. Then, the SnO_2 films were immersed into a 40 mM aqueous solution of $TiCl_4$ at 70 °C for 30 min and washed with water and ethanol, then sintered at 520 °C for 30 min. After cooling to 80 °C, the SnO_2 electrodes were put into 0.5 mM N719 dye ([Ru{LL′-(NCS)$_2$}], L = 2,2′-bipyridyl-4,4′-dicarboxylic acid, L = 2, 2′-bipyridyl-4, 4′-ditetrabutylammonium carboxylate, Solaronix) in ethanol, and was kept for 20 h at room temperature. The Pt-coated FTO counter electrode was prepared by dropping H_2PtCl_6 (5.0×10^{-4} M) solution on the FTO glass followed by heating at 400 °C for 15 min in air. The electrolyte consisted of 1-propyl-3-methylimidazolium iodide (PMII, 0.6 M), I_2 (0.03 M), LiI (0.05 M), guanidine thiocyanate (GuNCS, 0.1 M, Aldrich), and 4-tert-butylpyridine (0.5 M, Aldrich) in acetonitrile and valeronitrile (85:15 v/v). The active area of the dye-coated SnO_2 film was 0.16 cm^2, which was measured by profilometer (Ambios, XP-1).

Characterization: The phase purity of the products was characterized by powder XRD on a Bruker D8 Advance X-ray diffractometer using $Cu_{K\alpha}$ radiation (λ = 1.5418 Å). FE-SEM (JSM-6330F), transmission electron microscopy (TEM), high-resolution transmission electron microscopy (HRTEM), and selected-area electron diffraction (SAED) patterns were performed on a JEOL-2010 HR transmission electron microscope to characterize the morphology, size, and the intrinsic structure of the products. The N_2 adsorption–desorption isotherms of the hierarchical SnO_2 octahedra and nanoparticles were measured by using an ASAP 2010 surface-area analyzer (Micromeritics Instrument Corporation). UV/Vis diffuse reflectance spectra were measured on a UV/Vis–NIR spectrophotometer (UV, Shimadzu UV-3150). The adsorbed dye amounts were obtained by measuring the eluted dye concentration from the SnO_2 octahedra and nanoparticle films with the UV/Vis absorption spectroscopy. The thickness of the SnO_2 film was measured by using a profilometer (Ambios, XP-1). The current–voltage characteristics were analyzed by using a Keithley 2400 source meter under simulated AM 1.5 G illumination (100 mW cm^{-2}) provided by a solar simulator (69920, 1 kW Xe lamp, Oriel). The incident-light intensity was calibrated with a standard Si solar cell.

Acknowledgements

The authors acknowledge financial support from the National Natural Science Foundation of China (20873183, U0934003, J0730420), the Natural Science Foundation of Guangdong Province (8151027501000030), the Foundation of Sun Yat-Sen University, and the Open Foundation of the Shenzhen Key Laboratory of Special Functional Materials (2T0806), Shenzhen University, Shenzhen.

Keywords: compact layers · dye-sensitized solar cells · sonochemical synthesis · tin · tin oxide

[1] B. O'Regan, M. Grätzel, *Nature* **1991**, *353*, 737–740.
[2] M. Grätzel, *Nature* **2001**, *414*, 338–344.
[3] M. K. Nazeeruddin, F. De Angelis, S. Fantacci, A. Selloni, G. Viscardi, P. Liska, S. Ito, B. Takeru, M. Grätzel, *J. Am. Chem. Soc.* **2005**, *127*, 16835–16847.
[4] a) D. B. Kuang, J. Brillet, P. Cher, M. Takata, S. Uchida, H. Miura, K. Sumioka, S. M. Zakeeruddin, M. Grätzel, *ACS Nano* **2008**, *2*, 1113–1116; b) O. K. Varghese, M. Paulose, C. A. Grimes, *Nat. Nanotechnol.* **2009**, *4*, 592–597; c) M. Law, L. E. Greene, J. C. Johnson, R. Saykally, P. D. Yang, *Nat. Mater.* **2005**, *4*, 455–459.
[5] a) H. J. Koo, Y. J. Kim, Y. H. Lee, W. I. Lee, K. Kim, N. G. Park, *Adv. Mater.* **2008**, *20*, 195–199; b) D. H. Chen, F. Z. Huang, Y. B. Cheng, R. A. Caruso, *Adv. Mater.* **2009**, *21*, 2206–2210.
[6] a) Q. F. Zhang, T. P. Chou, B. Russo, S. A. Jenekhe, G. Z. Cao, *Angew. Chem.* **2008**, *120*, 2436–2440; *Angew. Chem. Int. Ed.* **2008**, *47*, 2402–2406; b) T. P. Chou, Q. F. Zhang, G. E. Fryxell, G. Z. Cao, *Adv. Mater.* **2007**, *19*, 2588–2592; c) C. X. He, B. X. Lei, Y. F. Wang, C. Y. Su, D. B. Kuang, *Chem. Eur. J.* **2010**, DOI: 10.1002/chem.201000264.
[7] D. B. Kuang, S. Ito, B. Werger, C. Klein, J. E. Moser, *J. Am. Chem. Soc.* **2006**, *128*, 4146–4154.
[8] F. Caruso, *Adv. Mater.* **2001**, *13*, 11–22.
[9] X. X. Xu, J. Zhuang, X. Wang, *J. Am. Chem. Soc.* **2008**, *130*, 12527–12527.
[10] a) A. Keys, M. Grätzel, *Chem. Mater.* **2002**, *14*, 2930–2935; b) J. F. Qian, P. Liu, Y. Xiao, Y. Jiang, Y. L. Cao, X. P. Ai, H. X. Yang, *Adv. Mater.* **2009**, *21*, 3663–3667; c) S. Gubbala, V. Chakrapani, V. Kumar, M. K. Sunkara, *Adv. Funct. Mater.* **2008**, *18*, 2411–2418.
[11] W. M. Zhang, J. S. Hu, Y. G. Guo, S. F. Zheng, L. S. Zhong, W. G. Song, L. J. Wan, *Adv. Mater.* **2008**, *20*, 1160–1165.
[12] X. G. Han, M. S. Jin, S. F. Xie, Q. Kuang, Z. Y. Jiang, Y. Q. Jiang, Z. X. Xie, L. S. Zheng, *Angew. Chem.* **2009**, *121*, 9344–9347; *Angew. Chem. Int. Ed.* **2009**, *48*, 9180–9183.
[13] H. G. Yang, H. C. Zeng, *Angew. Chem.* **2004**, *116*, 6056–6059; *Angew. Chem. Int. Ed.* **2004**, *43*, 5930–5933.
[14] C. H. Lu, L. M. Qi, J. H. Yang, X. Y. Wang, D. Y. Zhang, J. H. Xie, *Adv. Mater.* **2005**, *17*, 2562–2567.
[15] a) N. A. Dhas, K. S. Suslick, *J. Am. Chem. Soc.* **2005**, *127*, 2368–2369; b) K. S. Suslick, G. J. Price, *Annu. Rev. Mater. Sci* **1999**, *29*, 295–326; c) A. L. Morel, S. I. Nikitenko, K. Gionnet, A. Wattiaux, J. Lai-Kee-Him, C. Labrugere, B. Chevalier, G. Deleris, C. Petibois, A. Brisson, M. Simonoff, *ACS Nano* **2008**, *2*, 847–856.
[16] F. Fievet, J. P. Lagier, M. Figlarz, *MRS Bull.* **1989**, *14*, 29–34.
[17] X. L. Hu, J. M. Gong, L. Z. Zhang, J. C. Yu, *Adv. Mater.* **2008**, *20*, 4845–4850.
[18] a) A. Narayanaswamy, H. F. Xu, N. Pradhan, X. G. Peng, *Angew. Chem.* **2006**, *118*, 5487–5490; *Angew. Chem. Int. Ed.* **2006**, *45*, 5361–5364; b) J. P. Ge, Y. X. Hu, M. Biasini, W. P. Beyermann, Y. D. Yin, *Angew. Chem.* **2007**, *119*, 4420–4423; *Angew. Chem. Int. Ed.* **2007**, *46*, 4342–4345.
[19] S. Wohlrab, N. Pinna, M. Antonietti, H. Cölfen, *Chem. Eur. J.* **2005**, *11*, 2903–2913.
[20] a) S. Ito, P. Liska, P. Comte, R. Charvet, P. Péchy, U. Bach, L. Schmidt-Mende, S. M. Zakeeruddin, A. Kay, M. K. Nazeeruddin, M. Grätzel, *Chem. Commun.* **2005**, 4351–4353; b) K. Zhu, E. A. Schiff, N. G. Park, J. van de Lagemaat, A. J. Frank, *Appl. Phys. Lett.* **2002**, *80*, 685–687.
[21] H. J. Snaith, C. Ducati, *Nano Lett.* **2010**, *10*, 1259–1265.
[22] E. Scolan, C. Sanchez, *Chem. Mater.* **1998**, *10*, 3217–3223.

Received: February 5, 2010
Published online: June 30, 2010

